

**ANALYSIS OF THE FRAGMENTATION PROPERTIES OF QUARK AND
GLUON JETS AT THE CERN SPS $p\bar{p}$ COLLIDER**

UA1 Collaboration, CERN, Geneva, Switzerland

Aachen¹ - Amsterdam (NIKHEF)² - Annecy (LAPP)³ - Birmingham⁴ - CERN⁵ -
Harvard⁶ - Helsinki⁷ - Kiel⁸ - Queen Mary College, London⁹ - Padua¹⁰ -
Paris (Coll. de France)¹¹ - Riverside¹² - Rome¹³ - Rutherford Appleton Lab.¹⁴ -
Saclay (CEN)¹⁵ - Victoria¹⁶ - Vienna¹⁷ - Wisconsin¹⁸ Collaboration

G. Arnison¹⁴, M.G. Albrow¹⁴, O.C. Allkofer⁸, A. Astbury¹⁶, B. Aubert³, C. Bacci¹³,
J.R. Batley⁹, G. Bauer⁶, A. Bézaguet⁵, R.K. Bock⁵, E. Buckley⁹, M. Calvetti⁵,
P. Catz³, P. Cennini⁵, S. Centro¹⁰, F. Ceradini¹³, G. Ciapetti¹³, S. Cittolin⁵, D. Cline¹⁸,
C. Cochet¹⁵, J. Colas³, M. Corden⁴, D. Dallman¹⁷, D. Dau⁸, M. DeBeer¹⁵, M. Della Negra⁵,
M. Demoulin⁵, B. Denby¹⁴, D. Denegri¹⁵, D. Dibitonto⁵, A. DiCiaccio¹³, L. Dobrzynski¹¹,
J. Dorenbosch², J.D. Dowell⁴, R. Edgecock⁴, K. Eggert¹, E. Eisenhandler⁹, N. Ellis⁴,
P. Erhard¹, H. Faissner¹, M. Fincke Keeler¹⁶, P. Flynn¹⁴, G. Fontaine¹¹, R. Frey¹²,
R. Frühwirth¹⁷, J. Garvey⁴, S. Geer⁶, C. Ghesquière¹¹, P. Ghez³, K.L. Giboni¹, W.R. Gibson⁹,
Y. Giraud-Héraud¹¹, A. Givernaud¹⁵, A. Gonidec³, M. Goodman⁶, G. Grayer¹⁴, W. Guryn¹²,
T. Hansl-Kozanecka^{1,*}, W. Haynes¹⁴, L.O. Hertzberger², D. Hoffmann¹, H. Hofmann⁵,
D.J. Holthuizen², R.J. Homer⁴, A. Honma⁹, W. Jank⁵, G. Jorat⁵, P.I.P. Kalmus⁹,
V. Karimäki⁷, R. Keeler¹⁶, I. Kenyon⁴, A. Kernan¹², R. Kinnunen⁷, W. Kozanecki^{12,*}, D. Kryn¹¹,
P. Kyberd⁹, F. Lacava¹³, J.P. Laugier¹⁵, J.P. Lees³, H. Lehmann¹, R. Leuchs⁸, S. Levegrun⁸,
A. Lévêque^{5,15}, M. Levi⁵, D. Linglin³, E. Locci¹⁵, T. Markiewicz¹⁸, M. Markytan¹⁷,
T. Martin¹¹, G. Maurin⁵, T. McMahon⁴, J.-P. Mendiburu¹¹, O. Meyer⁵, T. Meyer⁵,
M.-N. Minard³, M. Mohammadi¹⁸, K. Morgan¹², M. Moricca^{5,13}, B. Mours³, Th. Muller⁵,
A. Nandi⁹, L. Naumann⁵, A. Norton⁵, L. Paoluzi¹³, F. Pauss⁵, C. Perault³, G. Piano Mortari¹³,
E. Pietarinen⁷, M. Pimiä⁷, D. Pitman¹², A. Placci⁵, J.-P. Porte⁵, E. Radermacher¹,
J. Ransdell¹², T. Redelberger¹, H. Reithler¹, J.P. Revol^{5,**}, J. Rich¹⁵, M. Rijssenbeek⁵, J. Rohlf⁶,
C. Roberts¹⁴, P. Rossi¹⁰, C. Rubbia⁵, G. Sajot¹¹, G. Salvini¹³, J. Sass^{5,15}, B. Sadoulet⁵,
A. Savoy-Navarro¹⁵, D. Schinzel⁵, W. Scott¹⁴, T.P. Shah¹⁴, I. Sheer¹², D. Smith¹², R. Sobie¹⁶,
M. Stenzler¹⁸, J. Strauss¹⁷, J. Streets⁴, K. Sumorok⁶, F. Szoncsó¹⁷, C. Tao¹¹, G. Thompson⁹,
J. Timmer⁵, E. Tscheslog¹, J. Tuominiemi⁷, B. van Eijk², P. Verecchia¹⁵, J.P. Vialle³,
J. Vrana¹¹, V. Vuillemin⁵, H.D. Wahl¹⁷, P. Watkins⁴, R. Wilke⁵, J. Wilson⁴, I. Wingerter³,
C.-E. Wulz¹⁷, T. Wyatt⁵, M. Yvert^{3,5}, and L. Zanello¹³

(Submitted to Nuclear Physics B)

*) Present address: SLAC, Stanford, Calif., USA.

**) Present address: MIT, Cambridge, Mass., USA.

ABSTRACT

A sample of two-jet events from the UA1 experiment at the CERN $p\bar{p}$ Collider has been used to study the fragmentation of high-energy quark and gluon jets into charged hadrons. Compared with lower-energy jets observed in e^+e^- and pp collisions, the fragmentation function measured in the present experiment is softer (i.e. peaked to smaller values of z) and the mean internal transverse momentum is larger, mainly because of the effects of the QCD scaling violations. Using our knowledge of the quark and gluon structure functions in the proton, together with the QCD matrix elements, a statistical separation of quark and gluon jets is achieved within the present experiment. The fragmentation function for the gluon jets is found to be softer, and the angular spread of the fragmentation products larger, than is the case for quark jets.

1. INTRODUCTION

Since the observation of jets at the SPS $p\bar{p}$ Collider [1], jet production properties have been extensively studied. At collider energy and over most of the range in jet transverse momentum (p_T) and pseudorapidity (η), gluon jets are expected to dominate over quark jets. In this paper, we show results on the fragmentation properties of jets in an inclusive way, hence dominated by gluons. Exploiting the difference in the shape of the structure functions for quarks and gluons, together with the appropriate QCD matrix elements, we perform a statistical separation of quark and gluon jets and study the fragmentation properties of each parton type separately.

2. DATA SAMPLE AND DEFINITIONS

2.1 Trigger and selection

This analysis is based on data collected in 1983 at $\sqrt{s} = 546$ GeV, with an integrated luminosity of 118 nb^{-1} . The data were taken using a single jet hardware trigger in the region $|\eta| \leq 3$, with three different thresholds (15, 20, 25 GeV/c) on the jet transverse momentum. To avoid trigger inefficiencies at large pseudorapidity, we have restricted our sample to the events where the trigger jet was in the very central part of the calorimetry: $|\eta(\text{jet})| \leq 1.4$. Only calorimetric information is used for defining the energy and direction of the jets. Details of the trigger, the jet-finding algorithm, and correction procedures have been given elsewhere [2].

In the present analysis a two-jet topology is selected, with the leading (p_T) jet having $p_T \geq 25$ GeV/c and with the two leading jets being back-to-back (within 30°) in the transverse plane. Fiducial cuts are applied to ensure good measurements of the jet energy in the calorimeter, and of the track momenta in the central drift chambers: we reject all jets close to the vertical plane (within $\pm 30^\circ$) in order to avoid gaps between the two halves of the calorimeters, and all jets close to the horizontal plane (within $\pm 30^\circ$) where the charged tracks are parallel to the magnetic field. We also reject the region $1.4 \leq |\eta(\text{jet})| \leq 1.7$, where the calorimeter geometry changes. A further cut $|\eta(\text{jet})| \leq 2.5$ is imposed to reduce the overlap with the spectator jets.

The hardware trigger has a limited angular aperture leading to a possible bias in the fragmentation properties of trigger jets. Furthermore the calorimeter gives an unequal response to hadronic and electromagnetic energy, such that jets passing the trigger threshold are preferentially rich in electromagnetic energy. To avoid any bias due to these effects, we have studied the fragmentation properties of jets opposite to trigger jets (so-called 'away jets'). In practice the final sample also included those trigger jets having p_T more than 15 GeV above the trigger threshold. While these jets are subject to trigger-bias effects, they constitute a small fraction ($< 3\%$) of the final sample and their inclusion introduces no significant overall bias. A requirement $p_T > 15$ GeV was imposed on the sample of away jets, eliminating $< 1\%$ of the final sample.

In this study of jet fragmentation we concentrate on the clean two-jet topology, which is the majority of events. If a third jet is present it will not affect the two-jet kinematics, provided its p_T is relatively low. Since one cannot distinguish between final-state bremsstrahlung and very wide fragmentation of one jet identified as two jets, we have only kept events where a third jet (if any) was likely to come from initial-state bremsstrahlung. We remove all events with $p_T^{3\text{rd}} \geq 0.2 \times [(p_T^{1\text{st}} + p_T^{2\text{nd}})/2]$, and all events with $|\cos \theta_3^*| \leq 0.8$, where θ_3^* is the angle of the third jet with the beam in the c.m.s. of the scattered partons. These cuts effectively remove the third jet close to one of the two leading jets, this jet being either a real third jet or an artificial splitting of one of the other two. After these cuts, 10,007 jets remain for analysis, in favourable acceptance regions and free of trigger biases.

2.2 Definitions

Our definition of the fragmentation variable z is: $z = p_t(\text{track})/p(\text{jet})$, where $p_t(\text{track})$ is the momentum component of a charged track along the jet axis, and $p(\text{jet})$ is the total jet momentum as determined from the vector sum of individual calorimeter cell energies. We associate charged tracks with jets by accepting any charged track within the cone of $\Delta R \leq 1$ around the jet axis from calorimetry {where $\Delta R = \sqrt{[\phi(\text{jet}) - \phi(\text{track})]^2 + [\eta(\text{jet}) - \eta(\text{track})]^2}$ }, provided the track also has $z \geq 0.01$. Only tracks associated with the vertex are included; a visual scan of the events shows that this represents a small loss in the charged multiplicity ($\leq 5\%$), which is taken into account in the acceptance correction. Internal transverse momenta p_t are defined as the momentum components of tracks perpendicular to the jet axis, in this case computed from associated charged tracks. In all studies, jets are considered independently of each other, except when defining the two-jet kinematics for the scaling variable Q^2 and for the gluon-quark discrimination.

3. INCLUSIVE JET PROPERTIES

3.1 Fragmentation function

We define the fragmentation function $D(z) = (1/N_{\text{jet}})(dN_{\text{ch}}/dz)$, where N_{ch} is the number of associated charged tracks as defined in subsection 2.2. The corrections applied on the raw fragmentation function are listed below.

- i) Charged tracks not associated with the hard-scattering process but associated with the jet by our prescription $\Delta R \leq 1$, will influence $D(z)$, contributing mostly at small z . To remove this background we consider a pseudojet axis far away from the true axis (at 90° in the transverse plane). A background fragmentation function is estimated around this axis (with the definition of subsection 2.2 to associate charged tracks), and the integrated background $D(z)$ distribution is subtracted from the original $D(z)$. At the lower z values ($z \lesssim 0.05$), this reduces the fragmentation function by $\approx 50\%$.
- ii) The non-uniform acceptance in ϕ of the central drift chamber, due to the orientation of the magnetic field, is corrected for by a z -independent jet azimuth-dependent correction (15% on the average).
- iii) The measured jet energy is corrected to take into account various losses due to the response of calorimeters and the limited opening of the association cone, which are only partly compensated by additional energy coming from the underlying event. These corrections have been determined [3] by Monte Carlo studies [4] and were found to be large: averaged over all jets the measured energy is $\approx 20\%$ lower than the true jet energy. This correction was not applied in our previous paper [2] and is responsible for an important ($\approx 20\%$ change on the slope) softening of $D(z)$.
- iv) Errors on the measurement of the track and jet momentum produce smearing of the fragmentation function $D(z)$. A weight is applied to each associated track and to each jet to correct for this effect, which was not taken into account previously [2].

We have checked the validity of these corrections with a full Monte Carlo simulation [4]. The corrected $D(z)$ is found to be the same as the generated $D(z)$ to within $\pm 10\%$.

In Fig. 1a and Table 1, we present the corrected fragmentation function $D(z)$ obtained from our data. The errors given are statistical only: systematic errors are discussed below. In Fig. 1a we also show the fragmentation function found in e^+e^- ($\sqrt{s} = 34$ GeV) [5] and pp ($\sqrt{s} = 63$ GeV) [6] collisions. A significantly softer fragmentation function is observed at the Collider, compared with the lower-energy data. This may be attributable to the change in QCD energy scale and to the different parton types in the samples. Our previously published result was obtained with less

statistical significance [2] and using a less sophisticated correction procedure. An empirical fit to the data [$D(z) = (3.4/z)e^{-7z}$] is also plotted (solid curve).

The systematic errors at low z are essentially due to the determination of the background. We have estimated this effect to be 20% of the value of the background estimate. The systematic errors at high z are dominated by the jet energy determination. This determination suffers from two very distinct problems: the absolute calibration of the calorimeters, and the validity of the energy correction described above. Since this energy correction is model-dependent, we have estimated the change on the value of the correction when adjusting the model to the data. The maximum expected change of this energy correction leads to an uncertainty of $\pm 5\%$ on the absolute energy scale. The absolute calibration of calorimeters introduces a further systematic error of $\pm 8\%$ on the jet energy scale. In Fig. 1b the fragmentation function $D(z)$ has been replotted. In this case the errors shown include both the statistical and systematic errors. The solid curve is a prediction [7] using a recent fragmentation model [8]. This model includes QCD evolution of parton showers and Lund string hadronization, and is in reasonable agreement with the data.

3.2 Fraction of charged jet energy

The fragmentation function obtained from charged tracks allows a simple estimate to be made of the average fractional energy of a jet carried by charged tracks; this is done by integrating $zD(z)$: $\int_{0.01}^1 zD(z)\Delta z = 0.44$. We have used the empirical fit of $D(z)$ to extrapolate the contribution of very soft particles ($z \leq 0.01$). For the final result this gives

$$\langle p_L^{\text{charged}}(\text{jet})/p(\text{jet}) \rangle = 0.47 \pm 0.02 (\text{stat.}) \pm 0.05 (\text{syst.}) . \quad (1)$$

The systematic error is dominated by the error on the jet momentum scale discussed above. The above result can be compared with the TASSO result [5]: 0.58 ± 0.02 . Given the size of our systematic errors, we do not consider this discrepancy to be significant.

3.3 Jet charged multiplicity

The average jet charged multiplicity N_{ch} can be obtained by integrating over $D(z)$. The result is dominated by the very low z contribution where uncertainties are very large. We prefer to remove this region and to estimate N_{ch} by using a model-dependent extrapolation. This extrapolation is most conveniently performed in terms of the relative rapidity $y = \frac{1}{2} \ln \left(\frac{E + p_\ell(\text{track})}{E - p_\ell(\text{track})} \right)$ in the laboratory frame, where E is the energy of a charged track assuming a pion mass. We have obtained the y distribution of all tracks within the jet cone of $\Delta R \leq 1$ in the jet hemisphere ($z \geq 0$). The background is determined at 90° to the jet in azimuth and subtracted. We have removed tracks with $y \leq 1.4$ and corrected for track losses as described in subsection 3.1.

In order to make a comparison of existing results, we have studied the variations of N_{ch} as a function of the two-jet mass m_{jj} . For a fixed two-jet mass bin, the y distribution is shown in Fig. 2a together with TASSO results at $W (= m_{\text{jj}}) = 34$ GeV. The beginning of the plateau is clearly visible for $1.5 \leq y \leq 2.0$. To estimate the multiplicity, we have chosen two reasonably extreme extrapolations of the plateau at $y = 0$. A lower estimate is given by the extrapolation of the fitted function (solid line) which also fits the TASSO data [5]. An upper estimate has been obtained by a flat extrapolation (dashed line) from the maximum in the rapidity distribution.

The dependence of the average jet charged multiplicity on the two-jet invariant mass is shown in Fig. 2b and Table 2. The full circles represent our results, where the lower and upper error bars correspond to lower and upper estimates; the open squares represent the results of this

method applied to the TASSO data of ref. [5]; the full line is the fit obtained by TASSO [5]. Our data are also in good agreement with the results of a similar analysis from UA2 [9] (open triangles) and seem to confirm the result that the jet charged multiplicity is almost independent of the two-jet mass in this range.

3.4 Transverse momenta relative to the jet axis

In this study the jet axis used was defined from the associated charged tracks. This choice is made in order to avoid a systematic overestimate of the relative p_t of charged tracks which may occur using the jet axis defined from the calorimetry. When plotting the average relative p_t as a function of the fragmentation variable z (Fig. 3a and Table 3), a correlation is observed (*seagull effect*) [2]. Also the results from TASSO [5] and R807 [6] are shown, indicating an overall increase of $\langle p_t \rangle$ at collider energy, although the shape of the curve looks similar to that at lower energy. The existence of such a correlation between z and p_t makes the average p_t strongly dependent on the cut applied in z . In Fig. 3b we show the p_t distribution $(1/N_{\text{jet}})(1/p_t)(dN_{\text{ch}}/dp_t)$ for two different cuts in z (for both figures the errors are only statistical). The corresponding average p_t values are $\langle p_t \rangle = 0.85 \pm 0.02$ GeV/c for $z \geq 0.1$, and $\langle p_t \rangle = 0.73 \pm 0.01$ GeV/c for $z \geq 0.05$. The systematic errors are due to the errors on the jet direction determination and are found to be $\sim 10\%$ with simulated events.

4. FRAGMENTATION OF QUARK AND GLUON JETS

4.1 Method

The gluon structure function of the proton is known to be considerably softer (i.e. peaked to smaller values of x) than the corresponding quark structure function. We exploit this difference to perform a statistical separation of quark and gluon jets. Our event selection allows the unambiguous calculation of the relevant kinematical quantities x_1 , x_2 , and \hat{s} , \hat{t} , \hat{u} [10], where \hat{s} , \hat{t} , and \hat{u} are the Mandelstam variables of the two-parton scattering process. Given the structure functions, we can therefore calculate, jet by jet, the probability that it is a gluon or quark jet. We define the probability P for the subprocess $ab \rightarrow cd$ to occur by

$$P(ab \rightarrow cd) = F_a(x_1, Q^2) \times F_b(x_2, Q^2) \times M^2(\hat{s}, \hat{t}, \hat{u})(ab \rightarrow cd) / \Sigma_{abcd} \text{ all subprocesses}, \quad (2)$$

where a , b , c , d are flavours, $F(x, Q^2)$ are the structure functions [11], and $M^2(\hat{s}, \hat{t}, \hat{u})$ are the relevant QCD matrix elements [12]. (When summing over initial flavour states, this formula becomes invariant for $\hat{u} \leftrightarrow \hat{t}$ exchange.) For each jet, we obtain the probability that it is a gluon jet from

$$P(\text{jet} = \text{gluon}) = \sum_{ab} P(ab \rightarrow \text{gluon} + \text{anything}). \quad (3)$$

The complement of the probability that a given jet originates from a gluon, $P(g)$, will be the quark probability $P(q) = 1 - P(g)$. If we calculate $P(g)$ for all jets in our sample, a signal is seen of events for which $P(q) \geq P(g)$. This signal corresponds to forward (large rapidity) jets, where it is expected that the probability of being a quark jet is enhanced.

We have removed indistinguishable configurations by imposing $|\cos \theta^*| \geq 0.25$ (where θ^* is the c.m.s. scattering angle). In order to separate clearly the effects of quark/gluon differences from the effects of scaling violations in the fragmentation properties, we have chosen to compare quark and gluon jets at the same value of $Q^2 \equiv 2\hat{s}\hat{t}\hat{u}/(\hat{s}^2 + \hat{u}^2 + \hat{t}^2)$. Although this definition is somewhat arbitrary it has the pragmatic advantage that it depends on the momentum transfer \hat{t} at fixed c.m.s. energy \hat{s} and therefore introduces an overlap in Q^2 between the quark-enriched and

the gluon-enriched samples [note that this definition of Q^2 is also used to calculate $P(g)$]. We have applied the following cut: $1600 \leq Q^2 \leq 2600 \text{ GeV}^2$ to avoid scaling violation effects (discussed in subsection 4.5).

The resulting $P(g)$ distribution is shown in Fig. 4. The two-humped structure of the distribution is an artefact of the kinematical cuts. We define gluon- and quark-enriched samples by $P(g) \geq 0.55$ and $P(q) = 1 - P(g) \geq 0.65$. If the distribution of any fragmentation variable (z for example) is measured in the gluon- and quark-enriched samples, an estimate of the pure gluon and quark z -distributions can be obtained by solving

$$\begin{aligned} d\sigma/dz &= \langle P(g) \rangle \times (d\sigma^{\text{gluon}}/dz) + [1 - \langle P(g) \rangle] \times (d\sigma^{\text{quark}}/dz), \\ d\sigma'/dz &= \langle P'(g) \rangle \times (d\sigma^{\text{gluon}}/dz) + [1 - \langle P'(g) \rangle] \times (d\sigma^{\text{quark}}/dz), \end{aligned} \quad (5)$$

where $d\sigma/dz$ and $d\sigma'/dz$ are the measured distributions in the enriched samples, and $\langle P(g) \rangle$ and $\langle P'(g) \rangle$ are the mean probabilities for a jet to be a gluon in these samples. The values corresponding to the cuts described above are: $\langle P(g) \rangle = 0.65$ for the gluon-enriched sample, and $\langle P'(g) \rangle = 0.17$ for the quark-enriched sample. The pure gluon ($d\sigma^{\text{gluon}}/dz$) and quark ($d\sigma^{\text{quark}}/dz$) distributions are calculated for each z bin.

4.2 Fragmentation function

In Fig. 5a we show the result of separating the gluon and quark fragmentation functions $D(z)$. The softer fragmentation for gluons, as expected from QCD, is indeed observed. We remark that a simple fit to the data gives $D(z)^{\text{gluon}} = (4.4/z) e^{-8.8z}$ for $\langle Q^2 \rangle = 2070 \text{ GeV}^2$, and $D(z)^{\text{quark}} = (3.4) e^{-6.9z}$ for $\langle Q^2 \rangle = 2060 \text{ GeV}^2$. This difference between quark and gluon is also shown in Fig. 5b (error bars are stat. + syst.) where the ratio of the two fragmentation functions is plotted. Also in Fig. 5b is shown the prediction from the model described above [7, 8].

The large error of 50% at very small z reflects the difficulties in correcting for soft background, especially for the quark-enriched sample. At high z , uncertainties on the jet energy corrections are the most important source of systematic errors. Assuming, as suggested by the data, that gluons fragment more softly than quarks, we have observed that jet energy corrections should be more important for gluon jets than for quark jets. We have checked that if the jet energy correction is proportional to $P(g)$ (full correction for pure gluon jets and half correction for pure quark jets, for example), the slope of the ratio is even steeper. Nevertheless, this change in the differences of fragmentation between quark and gluon jets is small compared with statistical errors, so that a second iteration on the jet energy correction was not considered necessary.

Also, a possible difference in the relative calibrations of the central (gluon jets) and forward (quark jets) calorimeters could contribute to the creation of artificial differences between the fragmentation of quark and gluon jets. We have checked, using the transverse momentum balance of the two leading jets, that such a systematic effect is small ($\leq 5\%$ of the jet transverse momentum). This effect is also small compared with the statistical errors. Thus we conclude that the effect we observe is not generated by systematic uncertainties on the jet energy scale.

4.3 Fraction of charged jet energy and charged multiplicity

Using the method described in subsection 3.2, we have obtained the charged energy fraction for quark and gluon jets separately: $\langle p_L^{\text{charged}}(\text{jet})/p(\text{jet}) \rangle^{\text{gluon}} = 0.50 \pm 0.04$ and $\langle p_L^{\text{charged}}(\text{jet})/p(\text{jet}) \rangle^{\text{quark}} = 0.44 \pm 0.04$, with an overall systematic error of 0.05. Within the statistical errors quoted above, the difference between the two measurements is not significant.

The method defined in subsection 3.3 can be used to determine the charged multiplicity of each sample. In practice, this determination is restricted to the gluon-enriched sample [$P(g) \geq 0.55$] since the quark-enriched sample suffers from very large systematic uncertainties at small z , as discussed previously. The result for the gluon-enriched sample [$\langle P(g) \rangle = 0.65$] is $N_{ch} = 12.2 \pm 0.6$ at a mean two-jet invariant mass of $95 \text{ GeV}/c^2$.

4.4 Internal transverse momentum and track flow

An analysis of the distribution of p_t relative to the jet axis, as explained in subsection 3.4, does not reveal any significant difference between gluons and quarks: $\langle p_t \rangle^{gluon} = 880 \pm 120 \text{ MeV}/c$ and $\langle p_t \rangle^{quark} = 850 \pm 140 \text{ MeV}/c$ for $z \geq 0.1$, with a systematic error of 10% for each result. The distribution of charged tracks $[(1/N_{jet})(1/\Delta R)(dN_{ch}/d\Delta R)]$ as a function of ΔR around the (calorimetric) jet axis is shown in Fig. 6 for quark and gluon jets separately. In this distribution, a difference is observed between quark and gluon jets: the gluon jets are wider than the quark jets. The systematic errors are small for this measurement and we consider this effect to be significant.

4.5 Scaling violation effects

Here we examine separately the effects of scaling deviations for quark and gluon jets. As, in practice, we are limited by the statistics of the quark-enriched sample, we study the fragmentation properties of a gluon-enriched sample [$P(g) \geq 0.5$] for different Q^2 intervals. In this comparison we can neglect the effects of quark/gluon differences because the mixture of quark and gluon jets is essentially the same for these Q^2 bins. We observe a clear Q^2 dependence: the fragmentation function appears to become softer (Fig. 7a) and the relative p_t larger (Fig. 7b) with increasing Q^2 . We want to stress that the scaling violation effects are more important than the quark/gluon differences. Thus it seems that the observed differences in the fragmentation properties compared with lower-energy experiments (Figs. 1a and 3a) are largely due to the effects of scaling violations rather than to quark/gluon differences.

In Fig. 7c we have plotted the extrapolated pure quark and gluon fragmentation function in bins of z versus two-jet mass, together with data obtained in TASSO [5]. Since the existing theoretical calculations [13] do not clearly establish the correct Q^2 scale for the fragmentation function itself, we have chosen for this comparison to plot all data sets as a function of the total c.m.s. energy squared (W^2 or m_{jj}^2) on grounds of simplicity. The full lines represent an empirical extrapolation made by the authors of ref. [5]. Our quark data are in somewhat better agreement with this extrapolation than are the corresponding gluon data.

4.6 Average jet charge

Using an event sample as described in subsection 4.1, but without the Q^2 cut and extending the separation method to probabilities that the jet originates from a certain quark flavour, we have measured some parameters related to the average jet charge. We have defined the charge of a jet with: $Q(\text{jet}) =$ the charge of the leading charged particle; $Q(\text{jet}) =$ the charge of the leading and next-to-leading charged particles; $Q(\text{jet}) = \sum_i Q_i z_i^{1/3}$. All definitions give the same numerical values within statistical errors. For example, with $Q(\text{jet}) = \sum_i Q_i z_i^{1/3}$, where i runs over all associated charged tracks, the following results are obtained:

Parton nature		$\langle Q(\text{jet}) \rangle$
enriched gluon	$[P(g) \geq 0.5]$	-0.03 ± 0.01 ,
enriched u-quark	$[P(u) \geq 0.5]$	$+0.15 \pm 0.03$,
enriched \bar{u} -quark	$[P(\bar{u}) \geq 0.5]$	-0.15 ± 0.03 .

The systematic errors are low (± 0.02), and we conclude that a non-zero charge is observed for quark (antiquark)-enriched jet samples, whereas the average charge of the gluon-enriched sample is compatible with zero.

With the above-quoted cuts applied on the probabilities, we can expect this asymmetry to be larger by a factor of 1.5 to 2 for pure samples: +0.22 to +0.30 for pure u-quarks for example. This number is consistent with the expectations of various models: ref. [14] gives +0.23 for $Q(\text{jet}) =$ the charge of the leading charged particle, and ref. [8] gives +0.33 for $Q(\text{jet})$ defined as in our results.

5. CONCLUSIONS

We have presented the fragmentation properties of jets at collider energy, and have observed results different to those published at lower \sqrt{s} values: our jets are broader and contain more charged tracks. A method for statistically separating gluon and quark jets has been devised, which results in significant differences between the quark and gluon jet samples: quark jets have a harder fragmentation and a higher degree of collimation. These observations are in agreement with the results obtained at lower energy [15]. Scaling violations are visible in the evolution of the distributions of the longitudinal and the transverse motion of the fragments and largely account for the differences observed with respect to the lower-energy data. An analysis of average jet charges demonstrates that gluon jets are neutral, whereas selected samples of u (\bar{u})-quark-enriched jets show a significant positive (negative) average charge.

Acknowledgements

We wish to thank G. Ingelman for his help with the Monte Carlo program and for numerous discussions.

We gratefully acknowledge the help of the management and the technical staff of CERN, and of all outside institutes collaborating in UA1. The following funding agencies in our home countries have contributed to this programme:

Fonds zur Förderung der Wissenschaftlichen Forschung, Austria.

Valtion luonnontieteellinen toimikunta Suomen Akatemia, Finland.

Institut National de Physique Nucléaire et de Physique des Particules, and

Institut de Recherche Fondamentale (CEA), France.

Bundesministerium für Forschung und Technologie, Fed. Rep. Germany.

Istituto Nazionale di Fisica Nucleare, Italy.

Science and Engineering Research Council, United Kingdom.

Department of Energy, United States of America.

The Natural Sciences and Engineering Council of Canada.

Thanks are also due to the following people who have worked with the Collaboration in the preparation of and data collection for the runs described here: F. Bernasconi, F. Cataneo, L. Dumps, D. Gregel, J.-J. Malosse, H. Muirhead, G. Stefanini, R. Wilson, Y.G. Xie and E. Zurfluh.

REFERENCES

- [1] M. Banner et al. (UA2 Collaboration), Phys. Lett. **118B** (1982) 203.
G. Arnison et al. (UA1 Collaboration), Phys. Lett. **123B** (1983) 115.
- [2] G. Arnison et al. (UA1 Collaboration), Phys. Lett. **132B** (1983) 223.
- [3] E. Buckley and W. Kozanecki, CERN UA1 technical note TN 85-08 (1985).
- [4] F. Paige and S.D. Protopopescu, ISAJET, BNL 31987 (1982).
- [5] K. Althoff et al. (TASSO Collaboration), Z. Phys. **C22** (1984) 307.
- [6] T. Åkesson et al. (AFS Collaboration), Z. Phys. **C30** (1986) 27.
- [7] P. Ghez and G. Ingelman, in preparation.
- [8] B. Andersson et al., Phys. Rep. **97** (1983) 31.
H.U. Bengtsson, G. Ingelman and T. Sjöstrand, The Lund Monte Carlo for QCD high-pt scattering, PYTHIA version 4.1 (1985).
T. Sjöstrand, Lund preprint, LU TP 85-10 (1985).
- [9] P. Bagnaia et al. (UA2 Collaboration), Phys. Lett. **144B** (1984) 291, Z. Phys. **C20** (1983) 117.
- [10] G. Arnison et al. (UA1 Collaboration), Phys. Lett. **136B** (1984) 294.
- [11] E. Eichten et al., Rev. Mod. Phys. **56** (1984) 579.
- [12] B.L. Combridge, J. Kripfganz and J. Ranft, Phys. Lett. **70B** (1977) 234.
- [13] R.K. Ellis et al., Nucl. Phys. **B173** (1980) 397.
- [14] R.D. Field and R.P. Feynman, Nucl. Phys. **B136** (1978) 1.
- [15] A. Petersen et al., Phys. Rev. Lett. **55** (1985) 1954.
M. Derrick et al., Argonne preprint ANL-HEP-PR/85-88 (1985).

Table 1

Distribution of the inclusive fragmentation function: $D(z) = (1/N_{\text{jet}})(dN_{\text{ch}}/dz)$
(errors are statistical only)

z	$D(z)$
0.015	186.4 ± 1.1
0.025	123.0 ± 1.0
0.035	86.0 ± 0.8
0.045	62.4 ± 0.7
0.055	46.5 ± 0.6
0.065	35.9 ± 0.5
0.075	29.1 ± 0.5
0.085	23.5 ± 0.4
0.095	18.4 ± 0.4
0.105	15.7 ± 0.4
0.115	12.4 ± 0.3
0.125	10.7 ± 0.3
0.135	9.66 ± 0.28
0.145	8.05 ± 0.26
0.155	6.95 ± 0.24
0.165	5.96 ± 0.22
0.175	4.92 ± 0.20
0.185	4.61 ± 0.19
0.195	4.22 ± 0.19
0.21	3.23 ± 0.12
0.23	2.46 ± 0.10
0.25	2.00 ± 0.09
0.27	1.68 ± 0.08
0.29	1.35 ± 0.08
0.32	1.02 ± 0.05
0.37	0.568 ± 0.029
0.43	0.331 ± 0.023
0.49	0.209 ± 0.019
0.56	0.125 ± 0.013
0.65	0.064 ± 0.009
0.75	0.025 ± 0.006
0.85	0.011 ± 0.005
0.95	0.008 ± 0.004

Table 2

Two-jet invariant mass m_{jj} dependence of the average jet charged multiplicity N_{ch}

m_{jj} (GeV)	N_{ch}
60–80	12.2 ± 0.2
80–100	12.0 ± 0.5
100–120	12.1 ± 1.0
120–160	12.4 ± 1.2

Table 3

z dependence of $\langle p_t \rangle$ of charged tracks relative to the jet axis (errors are statistical only)

z	$\langle p_t \rangle$ (MeV/c)
0.05 – 0.07	640 ± 10
0.07 – 0.10	690 ± 10
0.10 – 0.15	800 ± 10
0.15 – 0.20	850 ± 15
0.20 – 0.30	890 ± 15
0.30 – 0.40	990 ± 30
0.40 – 0.60	950 ± 30
0.60 – 1	830 ± 60

Figure captions

Fig. 1 The inclusive fragmentation function $D(z)$ (see text).

- a) UA1 result (full circles) $\langle m_{jj} \rangle = 95$ GeV (the errors plotted are statistical only); PETRA results (ref. [5]: TASSO $W = 34$ GeV, open squares); ISR result (ref. [6]: R807 $\langle m_{jj} \rangle = 29$ GeV, dashed line). The full line is a fit to the UA1 data: $D(z) = (3.4/z) e^{-7z}$.
- b) UA1 result (full circles); the errors plotted include the systematic error. The full line is the prediction of ref. [7].

Fig. 2 Rapidity distribution with respect to jet axis and the average jet charged multiplicity.

- a) Invariant rapidity distribution: $(1/N_{\text{jet}})(dN_{\text{ch}}/dy)$ for jets of $m_{jj} = 100, 120$ GeV (full circles). The solid line gives a lower estimate of the multiplicity, and the dashed line, an upper estimate. The fitted function for the lower-estimate case is of the form: $a \times e^{-by^{2/c}} \times \tanh(y-d)$. Open squares are TASSO data [5] for $W = 34$ GeV.
- b) Dependence of the average jet charged multiplicity on the effective mass m_{jj} of the two-jet system. Full circles are UA1 data with error bars for the lower and upper estimates; open squares are TASSO data extrapolated using the method described in the text; the full line is the $(\log s)$ fit to the TASSO data; and open triangles are UA2 data [9] (statistical errors only).

Fig. 3 The internal transverse momentum distribution and its dependence on z .

- a) The dependence of p_t on the longitudinal fragmentation variable z . Full circles are UA1 data (statistical errors only), open circles are TASSO data [5], and open squares are ISR data [6].
- b) Invariant relative p_t distributions for two different cuts in z and the $\langle p_t \rangle$ corresponding to each cut.

Fig. 4 The probability distribution for individual jets to be gluons. Indicated are the two cuts $[P(g) \leq 0.35$ and $P(g) \geq 0.55]$ used to define the quark- and gluon-enriched samples.

Fig. 5 Fragmentation functions $D(z)$ for quark-jets and gluon-jets separately (see text).

- a) Direct comparison of $D(z)$ for gluons and quarks (error bars are statistical only).
- b) Ratio of gluon/quark $D(z)$ as a function of z (error bars are stat. + syst.). Full line is from ref. [7].

Fig. 6 Charged track density as a function of ΔR (see text) for gluon and quark jets. This narrower profile of quark jets fully compensates the difference in fragmentation function (Fig. 5), so that no significant difference is observed in p_t between quark and gluon jets.

Fig. 7 The dependence of the fragmentation function $D(z)$ and of the p_t distribution on the two-jet system kinematics. The scaling variable Q^2 is discussed in the text. The distributions (a) and (b) are shown for a sample of enriched gluon jets $[P(g) \geq 0.5]$.

- a) $D(z)$ in two bins of Q^2 .
- b) p_t distribution in two bins of Q^2 , for $z \geq 0.1$.
- c) W^2 or m_{jj}^2 evolution of the fragmentation function per bin of z . Circles are from ref. [5]; squares are pure gluon jets and triangles are pure quark jets from UA1 data. The full lines represent a fit (ref. [5]) to the TASSO data.

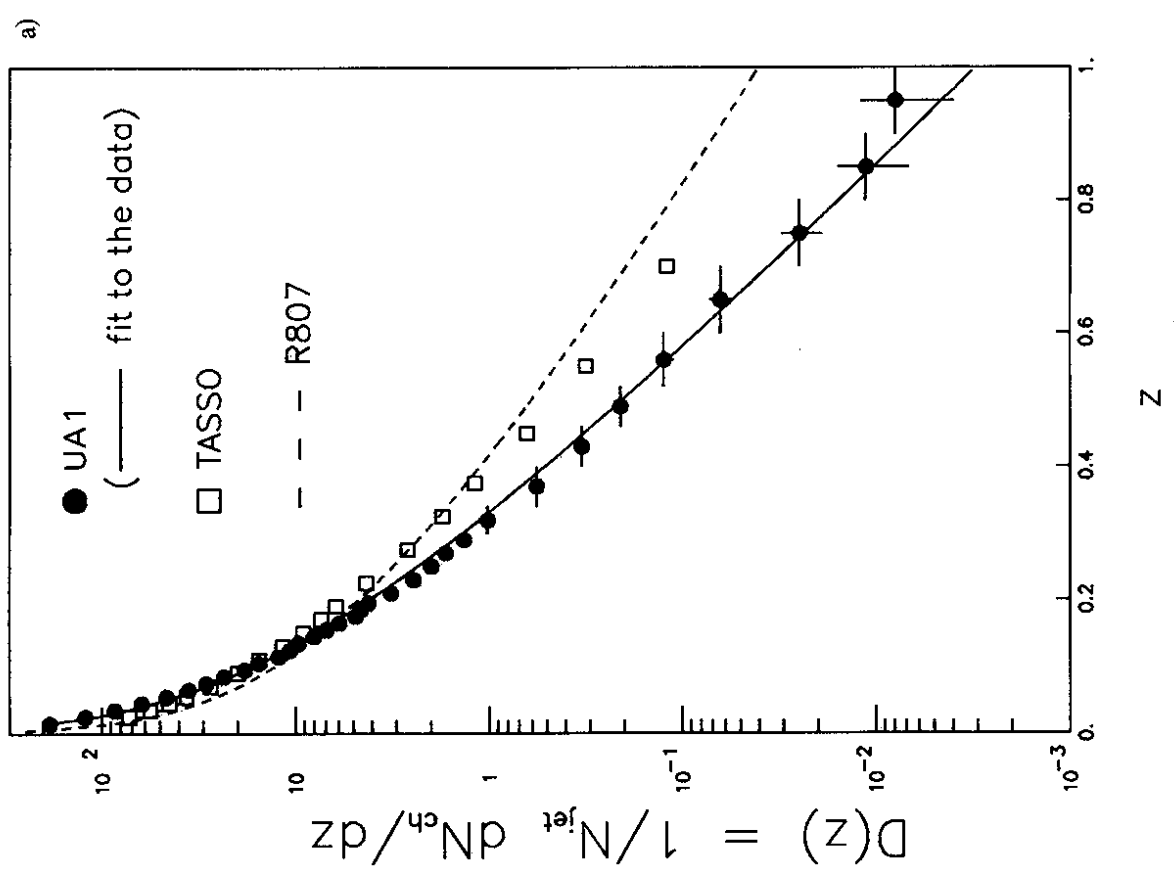
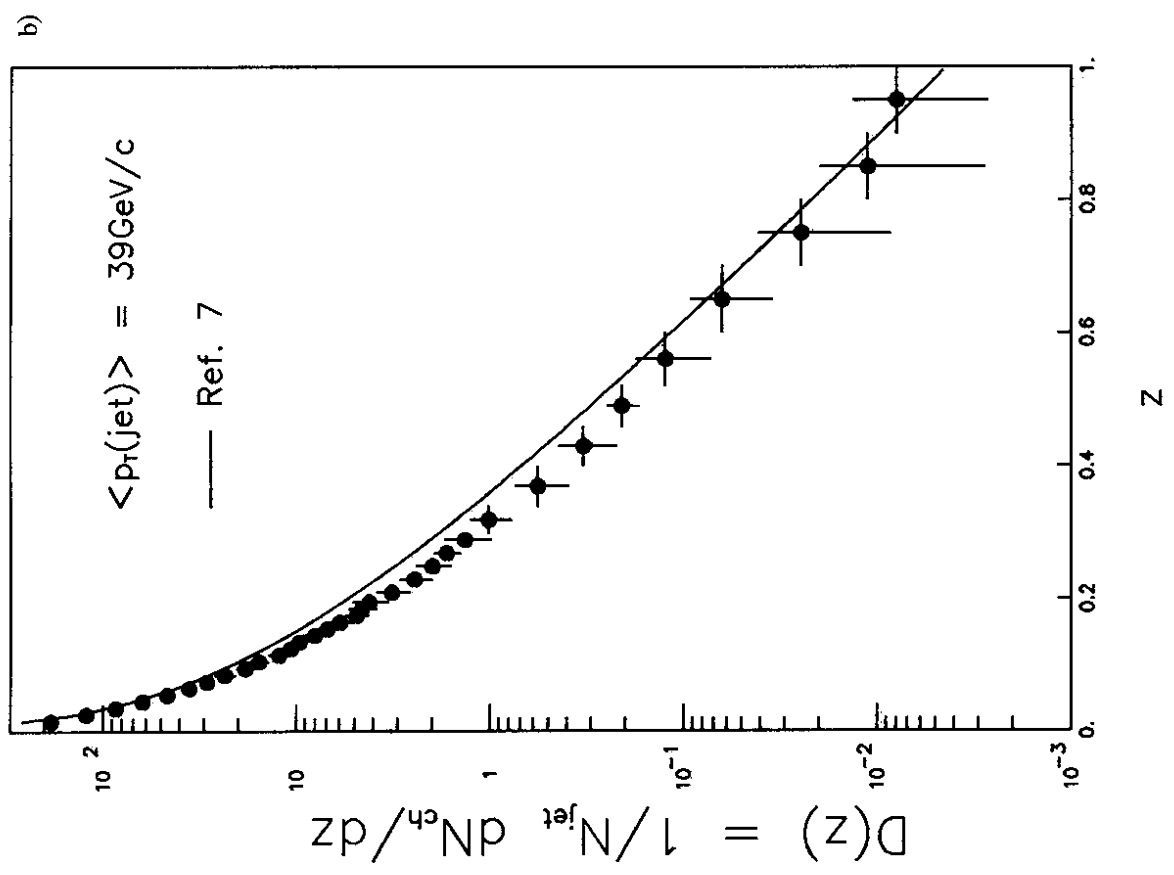


Fig. 1

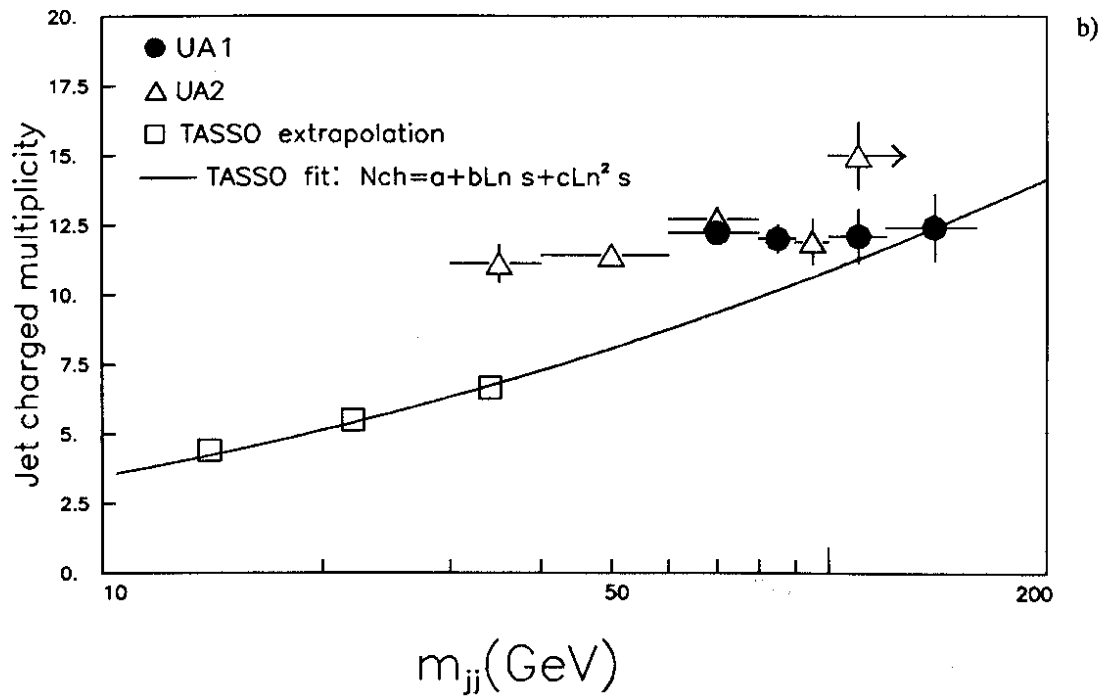
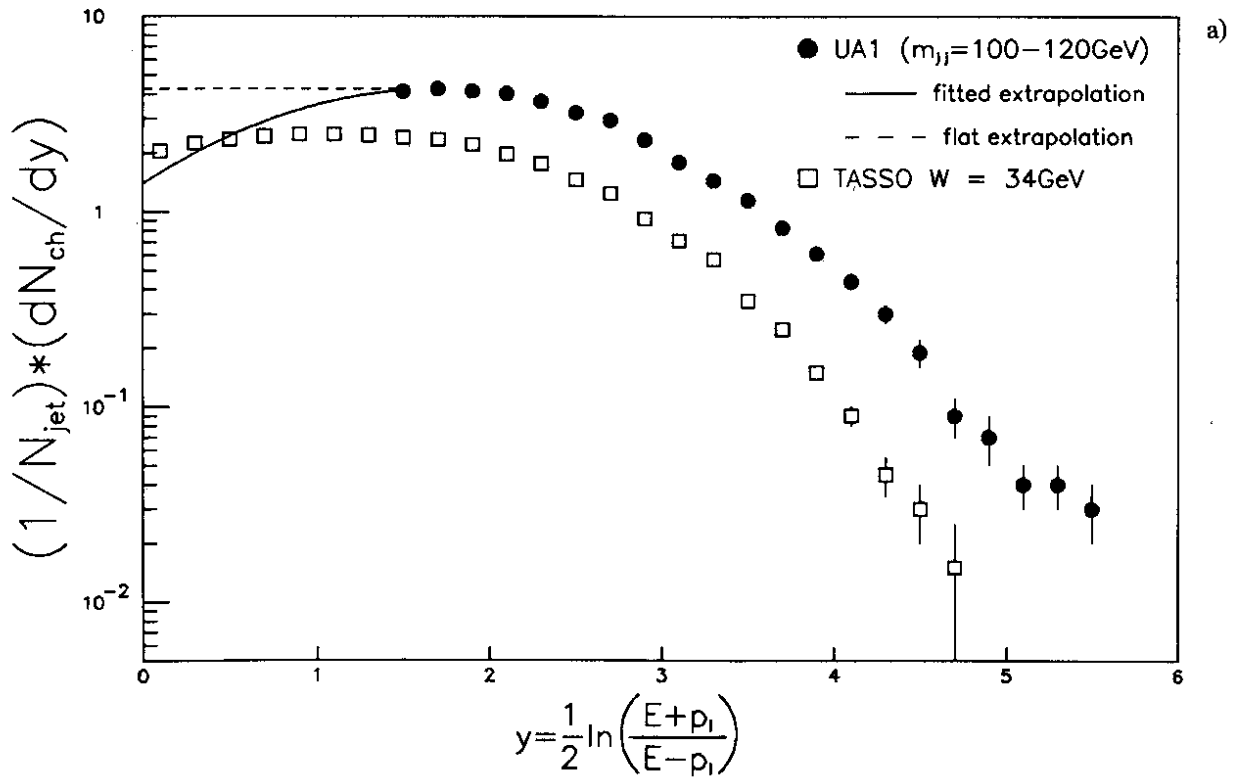


Fig. 2

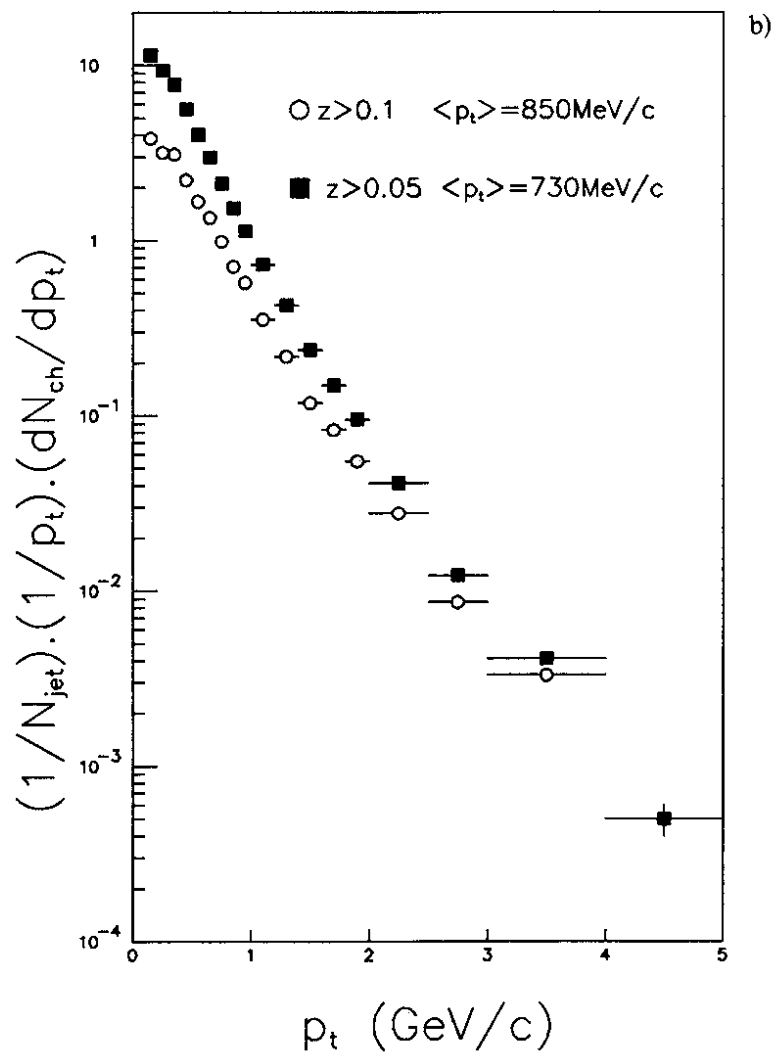
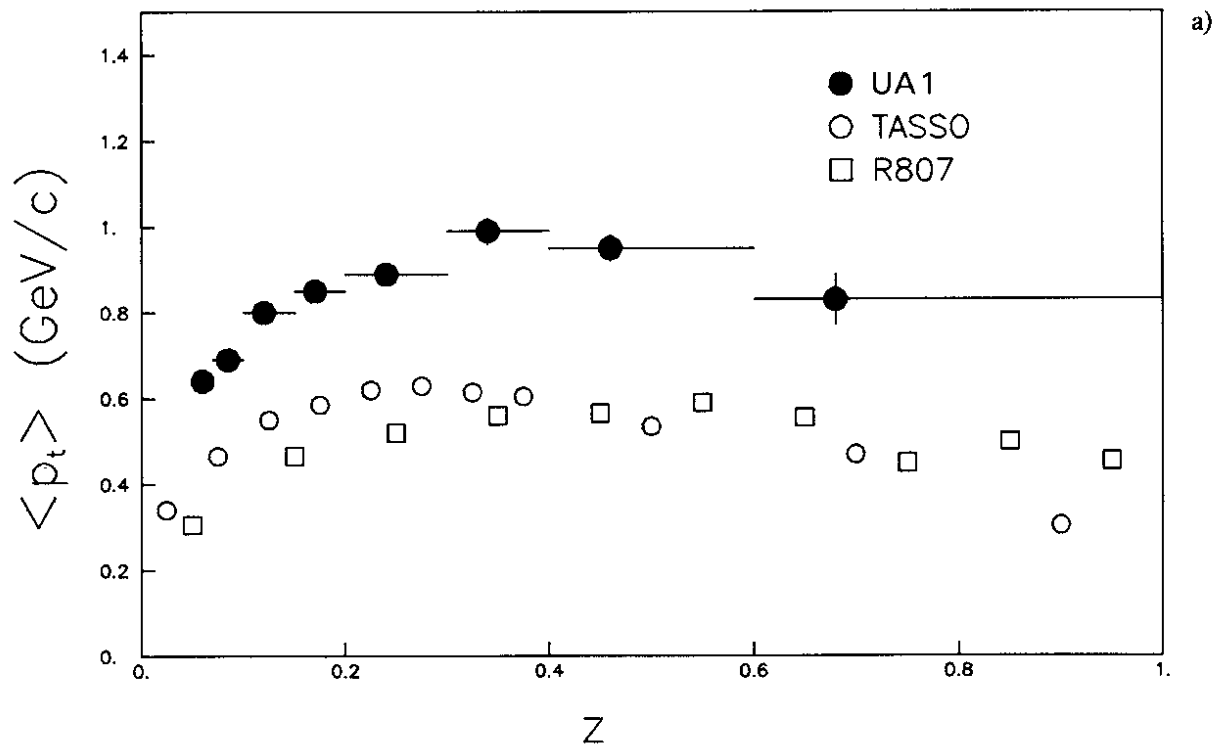


Fig. 3

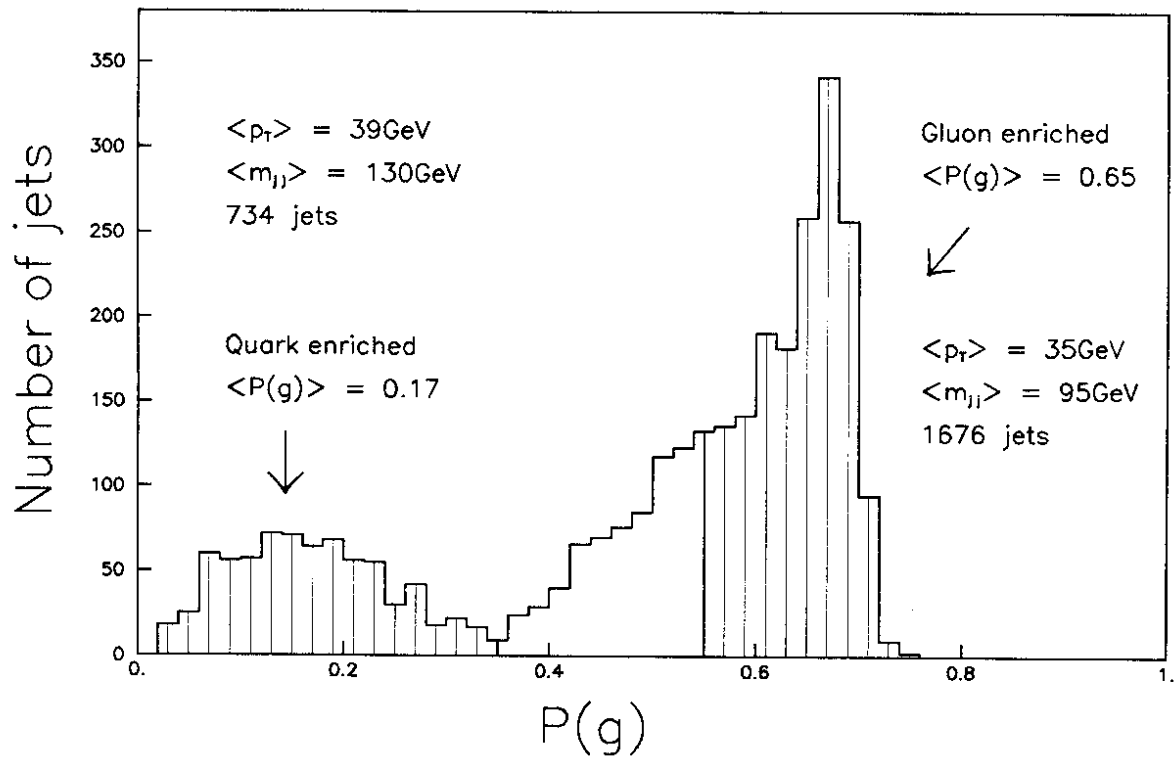


Fig. 4

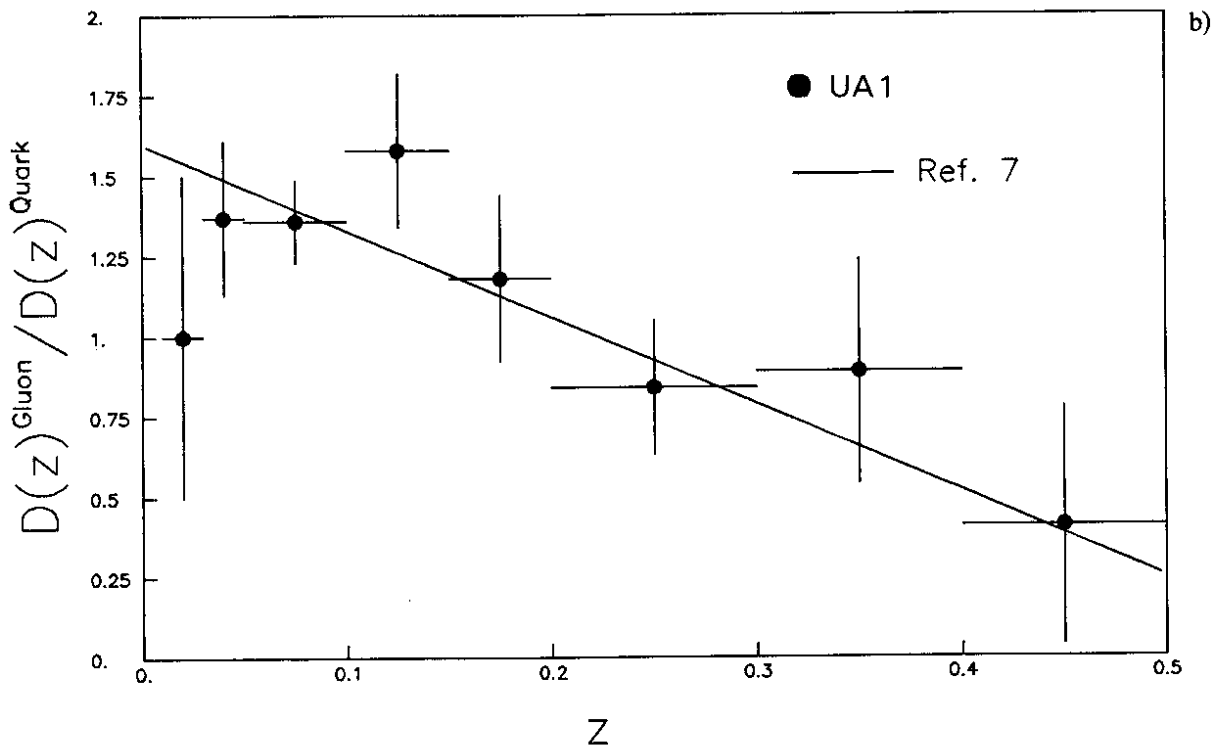
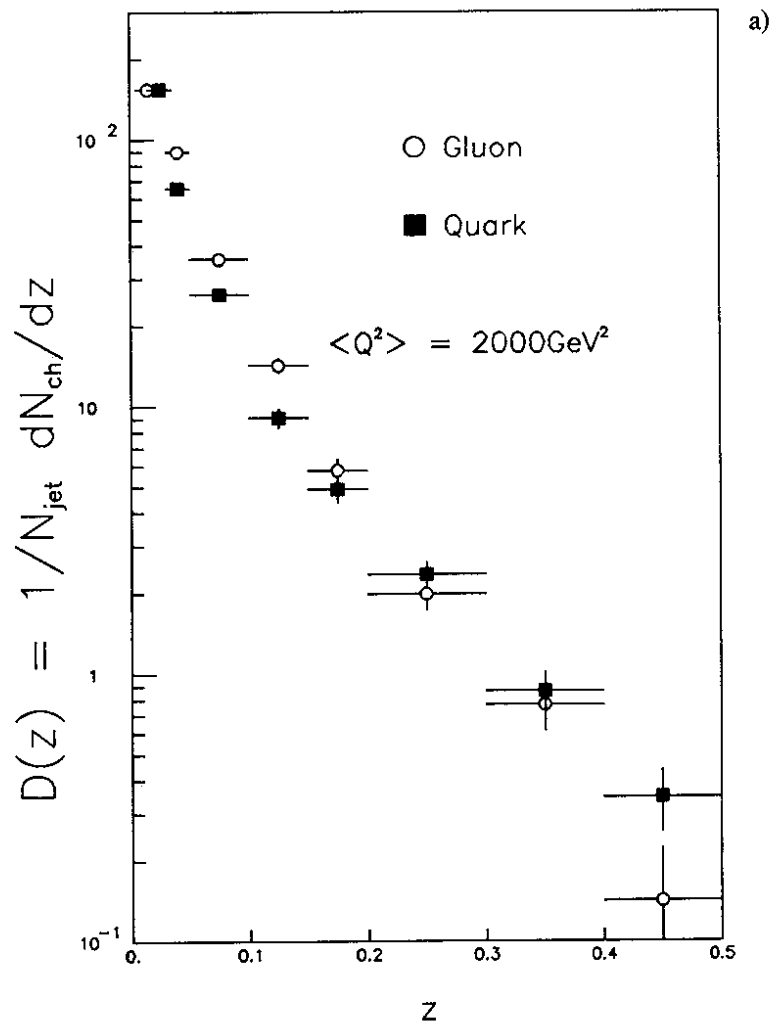


Fig. 5

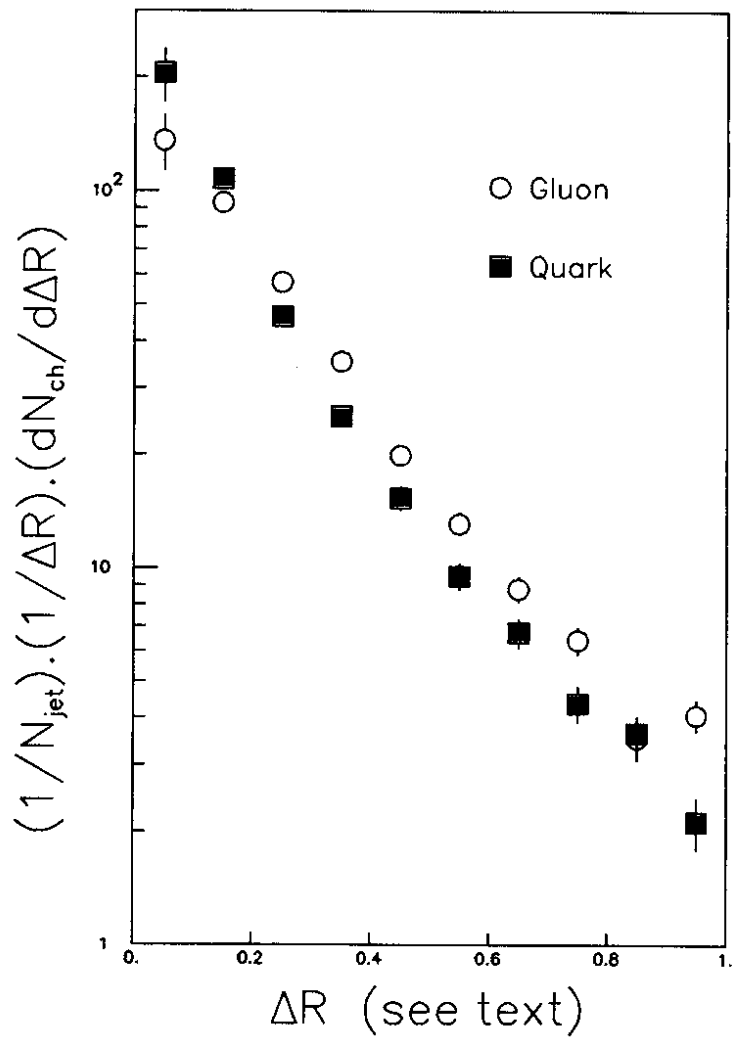


Fig. 6

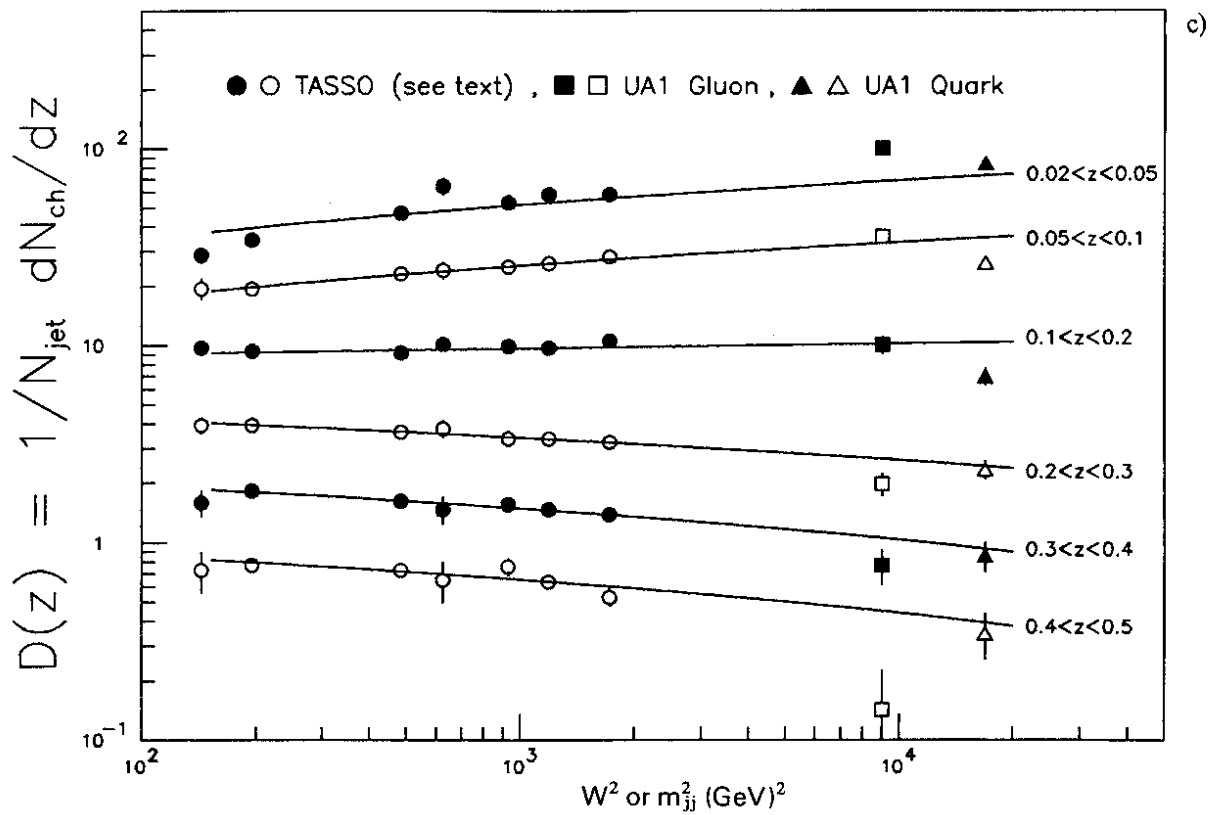
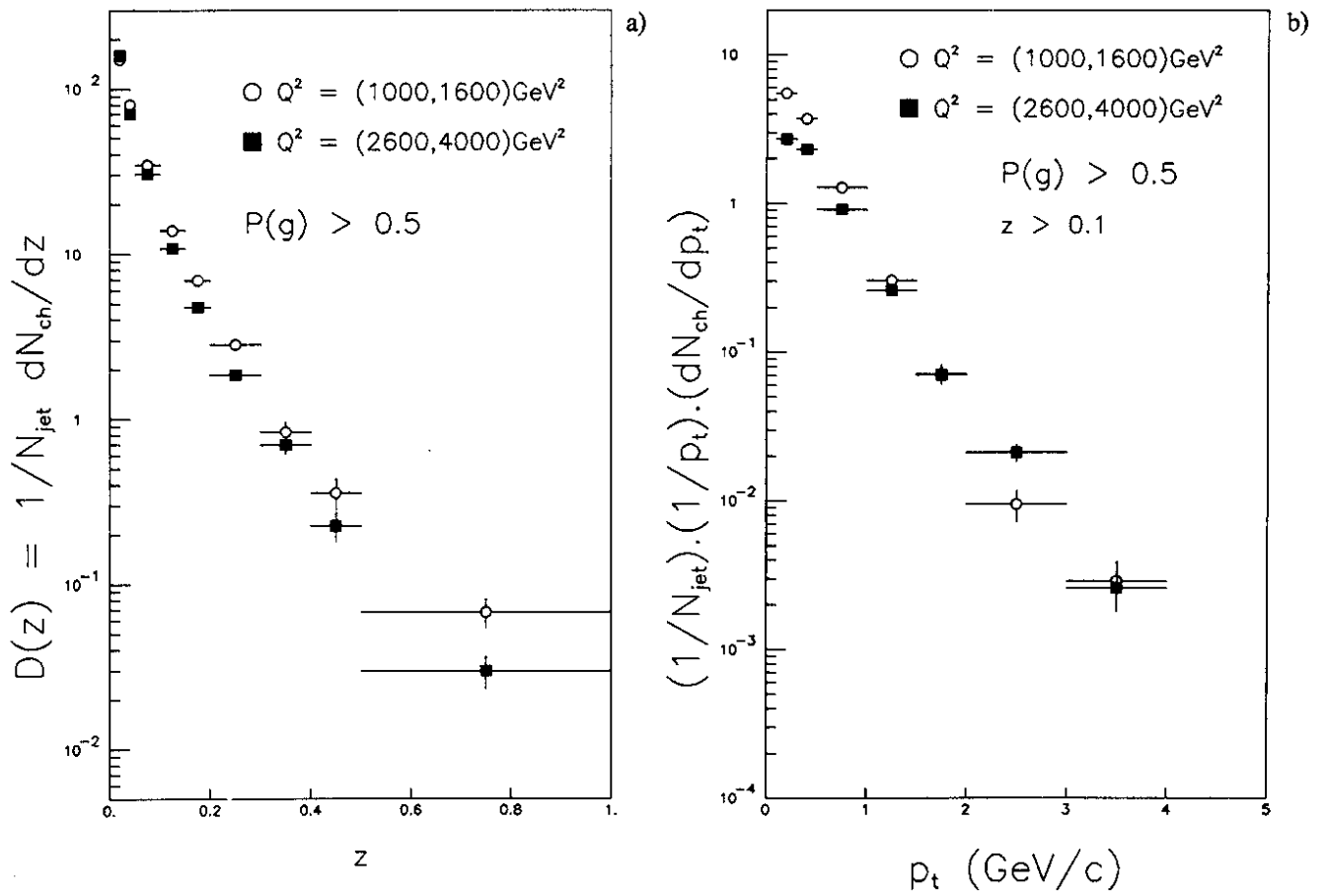


Fig. 7